Applied Catalysis B: Environmental 168-169 (2015) 458–464

Contents lists available at ScienceDirect

Applied Catalysis B: Environmental

journal homepage: www.elsevier.com/locate/apcatb

Photocatalytic CO_2 reduction with H_2O over $LaPO_4$ nanorods deposited with Pt cocatalyst

Bao Pan, Shijian Luo, Wenyue Su*, Xuxu Wang*

State Key Laboratory of Photocatalysis on Energy and Environment, Fuzhou University, Fuzhou 350002, PR China

ARTICLE INFO

Article history:
Received 11 November 2014
Received in revised form
23 December 2014
Accepted 27 December 2014
Available online 30 December 2014

Keywords:
CO_2 reduction
Photocatalysis
$LaPO_4$ nanorods
Pt cocatalyst

ABSTRACT

$LaPO_4$ nanorods synthesized by hydrothermal method were applied as a novel catalyst for photocatalytic reduction of CO_2 with H_2O under mild conditions (20 °C and 1 atm CO_2). The prepared $LaPO_4$ nanorods exhibited relatively negative E_{CB} of −0.63 V vs. NHE pH 7 and superior CO_2 adsorption capability of 16.3 mg g^{-1}. The yield rate of the main reduction products, CH_4 and H_2, were 0.11 and 0.08 μmol/h, respectively. The deposition of Pt cocatalyst improved the photocatalytic performance and enhanced the selectivity of CO_2 conversion to CH_4 production. The highest photocatalytic efficiency was observed over $LaPO_4$–1 wt%Pt, with an apparent quantum yield (AQY) enhanced by 5 times as compared to bare $LaPO_4$, and the selectivity for CH_4 production reached 100% at 3 wt%Pt loading. A possible mechanism of photocatalytic CO_2 reduction over $LaPO_4$ and $LaPO_4$–Pt was proposed that the Pt cocatalyst functioned as an excellent electron transfer mediator and adsorber for CO_2.

1. Introduction

The diminishing fossil resources and the growing concerns over the emissions of CO_2 have stimulated considerable research activities on the potential transformation of CO_2 [1,2]. The photocatalytic conversion of CO_2 using solar energy, i.e., the artificial photosynthesis, is one of the most attractive routes for the utilization of CO_2 [3]. The design of highly efficient and selective photocatalytic systems with the preferable utilization of solar energy through chemical storage is of vital interest, presenting the photocatalytic reduction of CO_2 with H_2O as one of the most desirable and challenging goals [4]. The photocatalytic production of CH_4 from CO_2 and H_2O has been reported on various semiconductor materials recently, such as TiO_2 [5–7], $La_2Ti_2O_7$ [8], $ZnGe_2O_4$ [9], and $ZnGa_2O_4$ [10], but with relatively low efficiency.

Semiconductors with a conduction band edge sufficiently more negative than the reduction potential of CO_2 with superior CO_2 adsorption capability are appropriate photocatalytic CO_2 reduction materials. Lanthanum-based materials possess a highly negative conduction band edge (−1.4 V vs. NHE) [11], which could be suitable for efficient reduction of CO_2 with H_2O to form hydrocarbon fuels. Some lanthanum-based compounds have been confirmed photocatalytic reduction activity for hydrogen production via water splitting [12–15]. In addition, alkaline lanthanum cation is considered as efficient CO_2 adsorption sites [16,17]. $LaPO_4$, an important member of the rare earth phosphate family, has been widely studied as luminescent materials in recent years [18–20]. The photogenerated carriers in $LaPO_4$ have relatively long lifetime as indicated by its high fluorescence efficiency. Moreover, the $LaPO_4$ colloid owns a high positive zeta potential of 32 mV (Fig. 1), which ensures the $LaPO_4$ nanoparticles effective dispersibility in aqueous media and favors CO_2 adsorption on the surface of $LaPO_4$ nanoparticles as CO_2 molecule has a positive electron affinity [21]. Therefore, the lanthanum-based $LaPO_4$, are expected to be promising candidates of photocatalysts for CO_2 reduction. So far the capability of $LaPO_4$ for catalyzing CO_2 reduction with H_2O under irradiation has not been reported.

In the present study, the $LaPO_4$ nanorods were prepared by hydrothermal method and used as photocatalysts for the reduction of CO_2 with H_2O under mild reaction conditions (20 °C and 1 atm CO_2) without any sacrificial reagents. The cocatalyst Pt was deposited on $LaPO_4$ surface in order to obtain higher effective and selective photocatalytic systems for the reduction of CO_2 with H_2O. The effects of Pt on the photocatalytic performance and physicochemical characterizations of $LaPO_4$ have been systematically investigated. The possible mechanism for the photocatalysis on the prepared $LaPO_4$ and $LaPO_4$–Pt samples under irradiation was proposed.

* Corresponding authors. Tel.: +86 591 83779105; fax: +86 591 83779105.
E-mail addresses: suweny@fzu.edu.cn (W. Su), xwang@fzu.edu.cn (X. Wang).

http://dx.doi.org/10.1016/j.apcatb.2014.12.046
0926-3373/

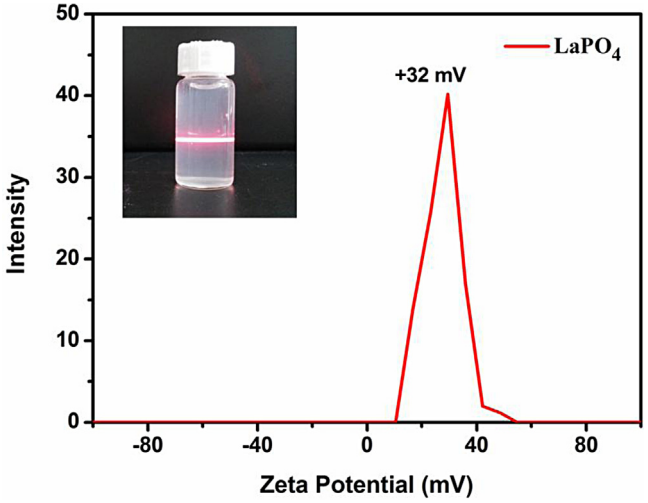

Fig. 1. Zeta potential (ζ) of LaPO4 aqueous dispersion (pH~7). Inset: $LaPO_4$ colloid image.

2. Experimental

2.1. Preparation of samples

$LaPO_4$ samples were synthesized by hydrothermal method. All reagents were of analytical purity and used without further purification. 3 mmol $La(NO_3)_3{\cdot}6H_2O$ and 3 mmol $(NH_4)_2HPO_4$ were dissolved in 35 mL of deionized water with stirring, respectively. Then $(NH_4)_2HPO_4$ solution was added into the $La(NO_3)_3$ solution dropwise under vigorous stirring. After stirring for 1 h, the mixture was transferred into a 100 mL Teflon liner. The autoclaves were heated at 180 °C for 24 h, and then cooled to ambient temperature naturally. The precipitates were washed with distilled water several times before it was dried at 60 °C to obtain the final product. $LaPO_4$–Pt samples were prepared via impregnating $LaPO_4$ powder in H_2PtCl_6 aqueous solution followed by $NaBH_4$ reduction [13].

2.2. Characterizations

The powder X-ray diffraction (XRD) was analyzed on a Bruker D8 Advance X-ray diffractometer. Scanning electron microscopy (SEM) images were collected on a Nova NanoSEM 230 microscopy (FEI Corp). Transmission electron microscopy (TEM) was obtained using a JEOL JEM 2010F microscope. Fourier transformed infrared (FTIR) spectra were recorded using a Nicolet Magna 670 FTIR spectrometer in KBr at a concentration of ca. 1%wt. UV–vis diffuse reflectance spectra (UV–vis DRS) were measured on a Varian Cary 500 Scan UV–vis-NIR spectrophotometer. Zeta potential of sample was determined by dynamic light scattering analysis (Zeta sizer 3000HSA) at 20 °C. X-ray photoelectron spectroscopy (XPS) measurements were performed on an ESCALAB 250 photoelectron spectroscope system. The Brunauer–Emmett–Teller (BET) specific surface area and CO_2 adsorption were measured with an ASAP2020M apparatus. Mott–Schottky measurement was performed with a Zennium electrochemical workstation (Zahner Elektrik, Germany), using Pt plate and Ag/AgCl electrode as the counter electrode and reference electrode, respectively. The working electrode was made by dip-coating catalyst slurry (5 mg·mL^{-1} in EtOH) on fluorine-doped tin oxide (FTO) glasses, the area of which was controlled as 0.25 cm^2, and followed by air-drying. 0.2 M of Na_2SO_4 solution was used as electrolyte.

2.3. Isosteric heat of adsorption (Q_{st}) calculations

According to Clausius–Clapeyron empirical equations that the data are modeled with a virial-type expression composed of parameters a_i and b_i that are independent of temperature: [22]

$$\ln P = \ln N + \frac{1}{T}\sum_{i=0}^{m} a_i N^i + \sum_{i=0}^{n} b_i N^i \quad (1)$$

where, P is pressure, N is the amount adsorbed (or uptake), T is temperature, and m and n determine the number of terms required to adequately describe the isotherm. For CO_2 adsorption, it is measured at 273 and 298 K using unity weights. The parameters a_i and b_i are achieved from global fitting of the 273 and 298 K data. Based on the above results, the isosteric heat of adsorption (Q_{st}) is calculated according to:

$$Q_{st} = -R\sum_{i=0}^{m} a_i N^i \quad (2)$$

where, R is the universal gas constant.

2.4. Photocatalytic activity measurements

The photocatalytic reduction of CO_2 was evaluated at 1 atm CO_2 partial pressure in a 200 ml reactor with an inner irradiation quartz reaction cell. The reactor was kept at 20 °C as controlled by cooling water. A 125 W high-pressure Hg lamp (GGZ125, Shanghai Yaming Lighting Co., Ltd with a maximum emission at about 365 nm) was used as light source. Typically 50 mg photocatalyst was suspended in 70 mL H_2O. Before irradiation, the whole reaction system was first evacuated by a mechanical pump to ensure the air was eliminated. Secondly, CO_2 (99.999% purity) was filled into the reactor for 1 h with stirring to get a CO_2-saturated aqueous solution. The gas products were analyzed by GC (Agilent 6890 N). The apparent quantum yield (AQY) is also measured under the same photocatalytic reaction conditions. The incident light intensity of high pressure mercury lamp is measured by SpectriLight ILT950. The total number of incident photons is measured using a calibrated silicon photodiode. The AQY is calculated according to the following Eqs.:

$$\mathrm{AQY}(\%) = \frac{\text{number of reacted electrons}}{\text{number of incident photons}} \times 100$$
$$= \frac{\text{number of}CH_4\text{ molecules} \times 8 + \text{number of } H_2 \text{ molecules} \times 2}{\text{number of incident photons}} \times 100 \quad (3)$$

3. Results and discussion

3.1. Photocatalytic performance of CO_2 reduction

The photocatalytic property of the prepared samples was carried out in the saturated CO_2 aqueous solution dispersing catalyst powers under mild conditions. In the control experiments no any gas but CO_2 was detected in the reaction system without irradiation or catalysts, indicating that the CO_2 reduction requires the procedure of photocatalysis. Besides, reduction product was only H_2 when the high purity N_2 replaced CO_2 in the reaction system. This result proved that the formed hydrocarbons were originated from CO_2 but not contamination.

CH_4 and H_2 are the two main reduction products. Fig. 2a and b displays the evolution of the reaction products generated from the $LaPO_4$ promoted CO_2 reduction system as a function of irradiation time. The generation of CH_4 and H_2 increases almost linearly with the irradiation time. After 5 h of irradiation, the accumulated yield of CH_4 and H_2 increases to 0.51 and 0.36 μmol, respectively, corresponding to the production rates of 0.11 and 0.08 μmol/h (Fig. 2c). Except for trace amount of CO, other products such as CH_3OH,

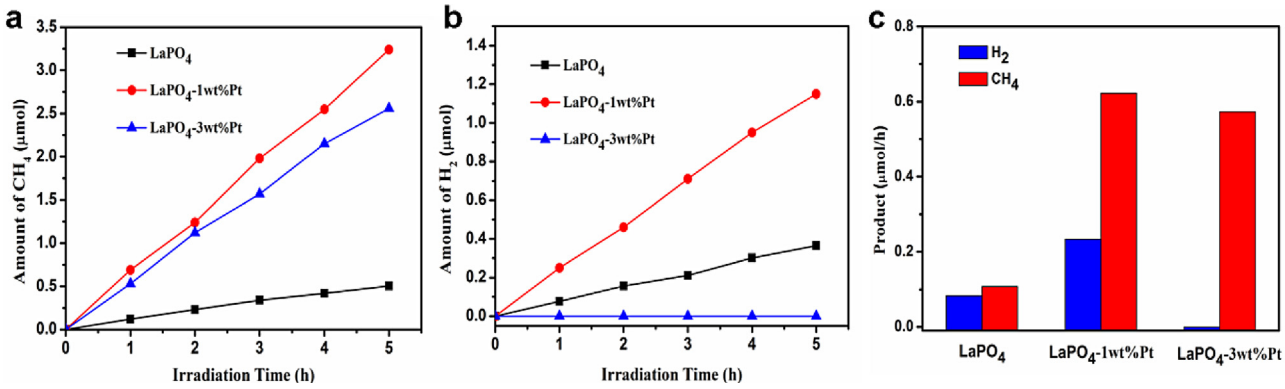

Fig. 2. Production of CH_4(a) and H_2(b) formed as a function of irradiation time, and (c) generation rates of CH_4 and H_2 over the prepared LaPO4 and $LaPO_4$–Pt samples.

HCHO, and HCOOH were not detected during the reaction. Taking the solubility of the potential reduced compounds into consideration, both insoluble CH_4 and H_2 are easy to overflow from the aqueous solution, while all of CH_3OH, HCHO, and HCOOH are soluble and difficult to separate from the reaction solution. So that the intermediates produced during the reduction tend to favor the formation of CH_4 and H_2 instead of CH_3OH, HCHO, and HCOOH. Furthermore, the strong oxidation power of photogenerated holes (or OH radicals) could react with those soluble intermediates and products of CO_2 conversion in reactions, [23] making the net yield negligible.

The photocatalytic activities for CO_2 reduction can be significantly enhanced by loading Pt as co-catalyst as shown in Fig. 2. The photocatalytic activity increases with increasing Pt content to a maximum at about 1 wt%, that the CH_4 and H_2 production rates reach the highest value of 0.62 and 0.23 μmol/h, respectively, which was 5.6 and 2.8 times as high as that of $LaPO_4$ (Fig. 2c). And the apparent quantum yield (AQY) is enhanced by 5 times. With the further increase of Pt content to 3 wt%, the lower CH_4-production rate is observed and no H_2 is detected, but the AQY is still 3.6 times higher than bare $LaPO_4$. Obviously, the platinization leads to an increase in the formation of CH_4 which is much superior to H_2 formation. As shown in Table 1, the selectivity for CH_4 production increases from the original 58.6% for $LaPO_4$ to 100% for $LaPO_4$–3 wt%Pt. Because both H_2 and CH_4 are formed via proton-assisted multielectron transfer reactions, and the formation of CH_4 (−0.24 V vs. NHE) is thermodynamically more feasible than the formation of H_2 (−0.41 V vs. NHE) when the supply of adsorbed CO_2, protons and electrons are high enough. The results of superior CH_4 selectivity indicate that the platinization would enhance both electron transfer and CO_2 adsorption in our proton-enriched system. Moreover, the repeated experiment is performed over $LaPO_4$–1 wt%Pt sample and the results show that there is no significant decrease in CH_4 and H_2 evolution rate after 4 times repeated reaction cycles (Fig. S1), indicating the good stability of $LaPO_4$–1 wt%Pt sample.

In order to evaluate the charge balance, the amount of O_2 formed during the photocatalytic CO_2 reduction was also quantified. For $LaPO_4$–1 wt%Pt sample, the amount of O_2 detected was 5.92 μmol after 5 h of reaction, and the amounts of H_2 and CH_4 formed were 1.15 and 3.24 μmol, respectively. Providing that the oxidation of H_2O to O_2 is the sole reaction to consume the photogenerated holes and that the photogenerated electrons are used for the formations of CH_4 and H_2, the stoichiometric molar ratio of $O_2/(4CH_4 + H_2)$ should be 1/2. The molar ratio of $O_2/(4CH_4 + H_2)$ calculated from our results is 0.42, which is close to the stoichiometric ratio.

Table 1
Effects of Pt cocatalyst on the photocatalytic activity and the selectivity of CO_2 reduction.[a]

Catalyst	CH_4 (μmol)	H_2(μmol)	$CH_4 + H_2$(μmol)	Sel.$_{CH4}$[b] (%)	AQY (%)
$LaPO_4$	0.51	0.36	0.87	58.6	0.03
$LaPO_4$–1 wt%Pt	3.24	1.15	4.39	73.8	0.15
$LaPO_4$–3 wt%Pt	2.56	0	2.56	100	0.11

[a] Reaction conditions: photocatalyst (50 mg), H_2O (70 mL), CO_2 pressure (1 atm), T (20 °C), irradiation time (5 h).
[b] $Sel._{CH4}(\%) = nCH_4/n_{(CH4+H2)} \times 100$.

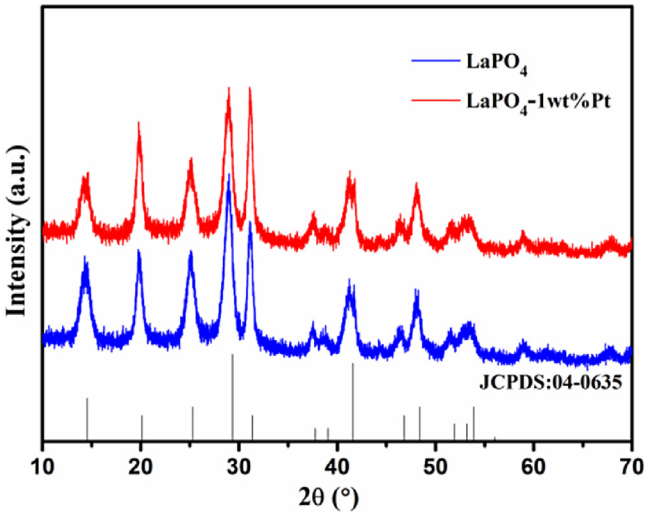

Fig. 3. XRD patterns of $LaPO_4$ and $LaPO_4$–1 wt%Pt samples.

3.2. Characterization of $LaPO_4$ and $LaPO_4$–Pt

The XRD patterns of $LaPO_4$ and $LaPO_4$–Pt samples are shown in Fig. 3. It is shown that all the diffraction peaks of the prepared $LaPO_4$ sample can be indexed to the hexagonal phase $LaPO_4$ (JCPDS: 04–0635) with lattice constants a = 7.04 Å, b = 7.04 Å, c = 6.45 Å. The strong and sharp diffraction peaks demonstrate high crystallinity of the products. The average crystal size of the sample is estimated to be about 11.5 nm from the (2 0 0) peak at around 29.0° by using the Scherrer equation. The diffraction peaks of $LaPO_4$–1 wt%Pt sample only ascribes to hexagonal phase $LaPO_4$. No diffraction peaks for Pt are observed in the $LaPO_4$–1 wt%Pt sample, which may owe to the low amount. FT-IR spectra of pure $LaPO_4$ and the $LaPO_4$–1 wt%Pt are shown in Fig. S2. No great difference can be found in the spectra of the two samples. The strong absorption peaks at 1022 cm^{-1} correspond to the asymmetric stretching (ν_3) vibration and the bands at 598 and 544 cm^{-1} are due to the asymmetric bending

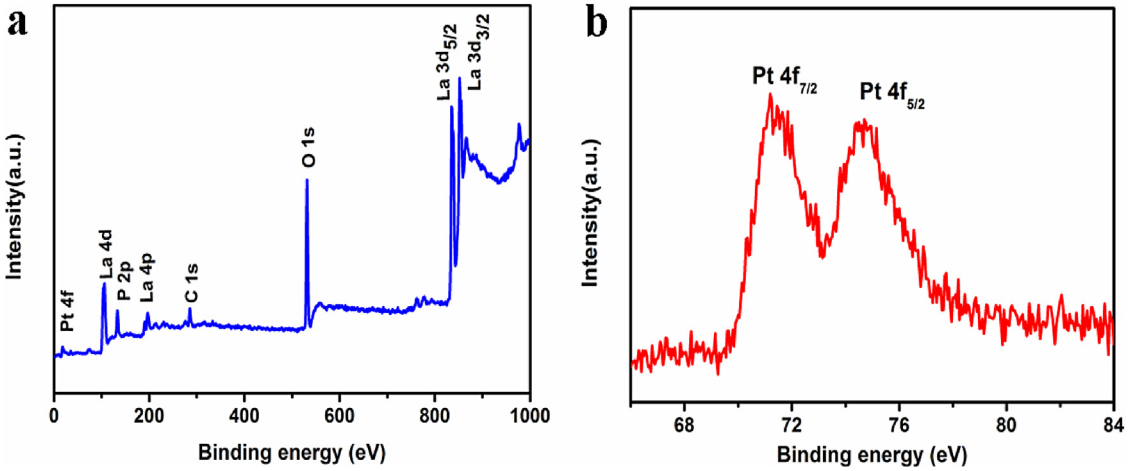

Fig. 4. XPS spectra of $LaPO_4$–1 wt%Pt sample: (a) survey spectra, (b) Pt 4f.

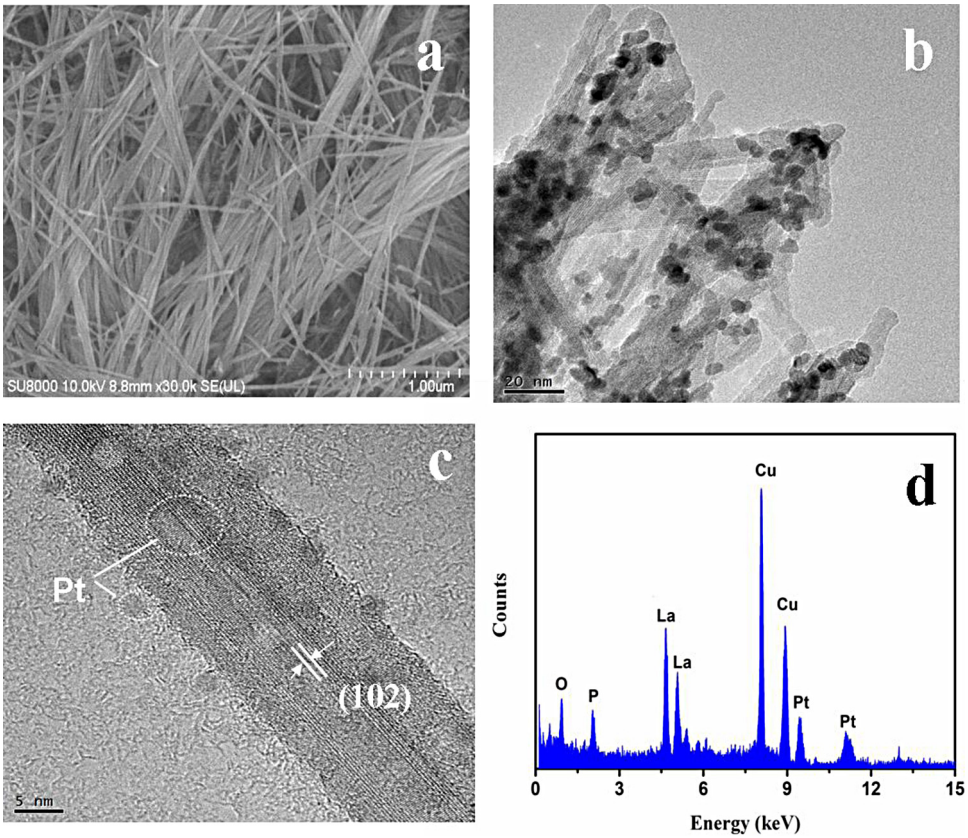

Fig. 5. (a) SEM image of the $LaPO_4$ sample; (b) TEM image, (c) HRTEM image, (d) EDX pattern of the $LaPO_4$–1 wt%Pt sample.

vibrations (ν_4) of -PO_4 group [24]. The absorptions at 3450 and 1620 cm^{-1} observed in the two samples can be assigned to the -OH stretching and H-O-H bending vibrations, respectively, of lattice water in pure $LaPO_4$ and $LaPO_4$–1 wt%Pt [25]. There are no other functional groups detected in these products. These results indicate that Pt deposition does not alter the phase and structure of $LaPO_4$.

The composition and chemical states of elements in the prepared samples were further investigated by X-ray photoelectron spectroscopy (XPS). The peak positions in all the XPS spectra were calibrated with C 1s peak at 284.60 eV. The survey XPS spectrum of the prepared $LaPO_4$–1 wt%Pt sample (Fig. 4a) indicates that the catalyst consists of La, O, P, and Pt, in accord with the result of EDX (Fig. 5d). Fig. 4b shows the Pt 4f XPS spectrum of the prepared sample. Two peaks emerging at binding energies of 70.9 and 74.4 eV correspond to Pt 4f7/2 and Pt 4f5/2, respectively, which indicates that Pt deposited on the $LaPO_4$ is metallic [26]. The XPS of La 3d (Fig. S3a) shows that the main peaks ($3d^04f^0$ configuration) of La 3d5/2 and La 3d3/2 at 835.1 and 851.9 eV with the shake-up peaks ($3d^04f^1$ configuration) located at 838.8 and 855.3 eV, respectively, correspond to La(III) oxidation state [27,28]. The peaks located at 133.6 eV of *P* 2p XPS (Fig. S3b) and 531.4 eV of O 1s XPS (Fig. S3c) are attributed to the P—O bonds in PO_4^{3-} chemical environment [29,30].

The structure and morphology of the samples were further characterized by SEM and HRTEM. As shown in the SEM (Fig. 5a), the prepared $LaPO_4$ sample consists of straight, smooth, and homogeneous nanorods with a uniform diameter of about 16 nm

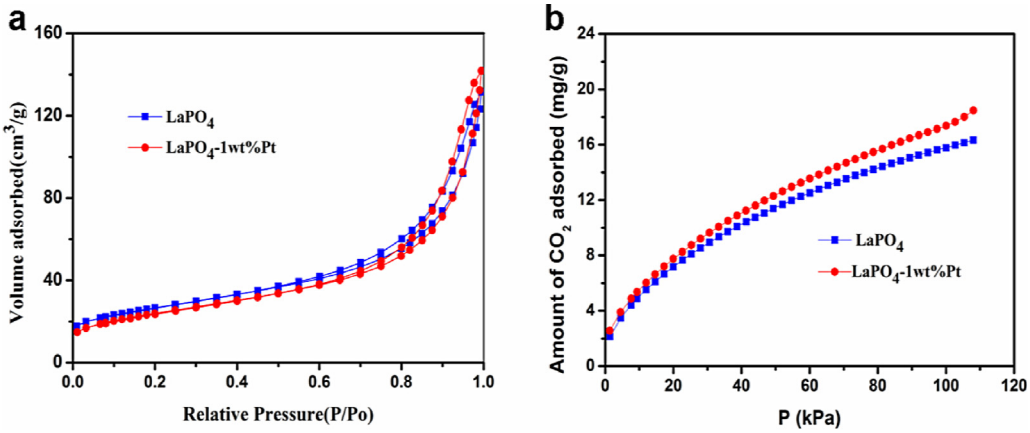

Fig. 6. (a) N_2 adsorption/desorption isotherms (77 K), and (b) CO_2 adsorption isotherms (1 atm, 273 K) of $LaPO_4$ and $LaPO_4$–1 wt%Pt samples.

Table 2
The S_{BET}, the CO_2 adsorbed amounts, and the isosteric heat of CO_2 adsorption (Q_{st}) on $LaPO_4$ and $LaPO_4$–1 wt%Pt samples.

Catalyst	S_{BET}($m^2 \cdot g^{-1}$)	CO_2adsorbed amounts ($mg \cdot g^{-1}$)	Q_{st}(kJ/mol)
$LaPO_4$	110	16.3	31.52
$LaPO_4$–1 wt%Pt	104	18. 5	27.25

and length of up to several tens micrometers. The TEM of the $LaPO_4$–1 wt%Pt sample (Fig. 5b) shows the existing of numerous randomly organized one-dimensional nanorods with surface deposition of irregular Pt nanoparticles with a diameter of about 3–7 nm. The HRTEM image of $LaPO_4$–1 wt%Pt (Fig. 5c) shows that the Pt nanoparticles on the $LaPO_4$ nanorods are well distributed and the lattice spacing of $LaPO_4$ is 0.285 nm, corresponding to the (1 0 2) planes. The obtained EDX pattern corresponding to Fig. 5d shows that the sample is composed of La, P, O, and Pt elements (Cu peaks arise from TEM grid).

The BET specific surface area (S_{BET}) of as-prepared $LaPO_4$ and $LaPO_4$–1 wt%Pt was measured to be 110 and 104 $m^2\,g^{-1}$, respectively (Fig. 6a). The decrease in S_{BET} can be accounted for the partial surface coverage of $LaPO_4$ by the deposited Pt nanoparticles [31]. However, the CO_2 adsorption amounts increase from the original 16.3 $mg\,g^{-1}$ for $LaPO_4$ to 18.5 $mg\,g^{-1}$ for $LaPO_4$–1 wt%Pt (Fig. 6b). There is no significant difference in the CO_2 adsorption between $LaPO_4$ photocatalysts treated with $NaBH_4$ or not, which suggests the Pt cocatalysts work as CO_2 adsorption sites, excluding the effect of $NaBH_4$ reduction, just as the report that the Pt(1 0 0) surface prefers CO_2 adsorption by (thh) site [32]. Moreover, the calculated isosteric heat of CO_2 adsorption (Q_{st}) on $LaPO_4$–1 wt%Pt sample is lower than that on bare $LaPO_4$ (as listed in Table 2), indicating that the loaded Pt cocatalyst functions as CO_2 adsorption sites. Both the larger CO_2 adsorption amount and lower isosteric heat of CO_2 adsorption on $LaPO_4$–1 wt%Pt sample lead to higher CO_2 reduction activity.

In order to better understand the intrinsic electronic properties of $LaPO_4$ and $LaPO_4$–Pt samples, the band structure of $LaPO_4$ has been evaluated based on the combination of the flat-band potential and band gap [33]. As shown in Fig. 7, the flat-band potential of $LaPO_4$ determined from Mott–Schottky plots is ca. −0.73 V vs. Ag/AgCl at pH 7 (equivalent to −0.53 V vs. NHE at pH 7). Pt deposition does not alter the flat-band potential of $LaPO_4$ as that the Mott–Schlttky plots of $LaPO_4$ and $LaPO_4$–1 wt%Pt are found to converge to a common point on the potential axis (Fig. 7). It is found that the slopes of the plots are positive, suggesting that $LaPO_4$ is *n*-type semiconductor [34]. For *n*-type semiconductor, the conduction band lies very close to the flat-band potentials [35]. Therefore, the redox potential of conduction band (E_{CB}) of $LaPO_4$ is −0.63 V vs. NHE at pH 7. The band gap of the as-prepared $LaPO_4$ was determined from the UV–vis absorption spectrum (Fig. S4) to be 4.5 eV. So the edge of the valence band E_{VB} of $LaPO_4$ is calculated to be 3.87 V vs. NHE at pH 7, which is more positive than $E^{\theta}(H_2O/O_2)$ (0.82 V vs. NHE at pH 7). This indicates that holes photogenerated on irradiation of $LaPO_4$ can react with H_2O to produce O_2.

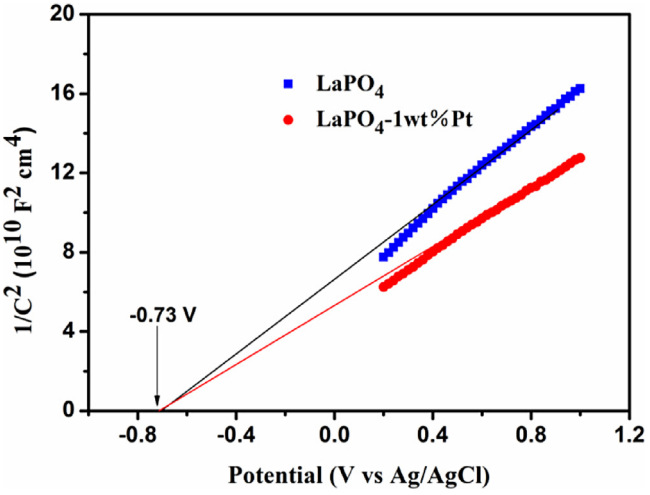

Fig. 7. Mott–Schottky plots of the prepared $LaPO_4$ and $LaPO_4$–1 wt%Pt samples.

Fig. 8a shows the transient photocurrent responses under intermittent UV–vis illumination. It is clearly seen that, with the introduction of Pt, the transient photocurrents of $LaPO_4$–1 wt%Pt sample are remarkably higher than that of bare $LaPO_4$, suggesting the more efficient separation and longer lifetime of photogenerated charge carriers [36] than that of bare $LaPO_4$. Fig. 8b shows the photoluminescence (PL) spectra of the $LaPO_4$ and $LaPO_4$–1 wt%Pt samples. Two distinct emission bands at 355 and 443 nm are observed due to the d–f transition of La^{3+} ions [37]. The PL intensity obtained from $LaPO_4$–1 wt%Pt is diminished as compared to that of $LaPO_4$, demonstrating the more efficient inhibition of charge carriers recombination in the $LaPO_4$–1 wt%Pt sample, and thus reflecting the superior electron transfer ability of Pt cocatalyst, which is consistent well with the results of the transient photocurrent responses. All the observations highlight the function of Pt cocatalyst for enhancing charge transfer, leading to the higher photocatalytic efficiency.

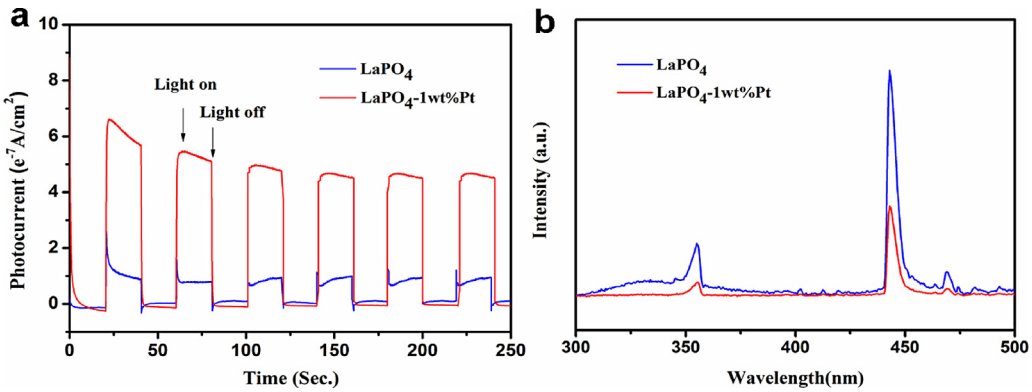

Fig. 8. (a) The transient photocurrent responses with an applied potential of +0.1 V, and (b) the photoluminescence (PL) spectra under 270 nm excitation of $LaPO_4$ and $LaPO_4$–1 wt%Pt samples.

3.3. Proposed mechanism

Based on the results of the above reaction and characterizations, we propose the mechanism of CO_2 reduction with H_2O over $LaPO_4$. When light with photon energy higher or equal to the band gap of $LaPO_4$ is incident on the catalyst, electrons and holes are generated in the CB and VB, respectively. (Eq. (4)) The CB edge, which is mainly formed by the La 5d states [38], has a higher energy level than CO_2/CH_4 and H_2/H_2O potential, thus the photogenerated electrons on the CB are transferred to the absorbed CO_2 and H^+ to produce CH_4 or H_2 (Eqs. (5) and (6)). While the VB edge of $LaPO_4$, mainly formed by the O 2p states [38], is positive enough to oxidize water. (Eq. (7))

$$LaPO_4 + h\upsilon \rightarrow h^+ + e^- \quad (4)$$

$$CO_2 + 8H^+ + 8e^- \rightarrow CH_4 + 2H_2O \quad (5)$$

$$2H^+ + 2e^- \rightarrow H_2 \quad (6)$$

$$2H_2O + 4h^+ \rightarrow O_2 + 4H^+ \quad (7)$$

The Pt nanoparticles deposited on the $LaPO_4$ is a key factor for the photocatalytic CO_2 reduction, which influences the efficiency and the selectivity of photocatalytic CO_2 conversion. With the high electrical conductivity of the deposited Pt and the abundant Schottky barriers formed at the interface between $LaPO_4$ and Pt, the deposited Pt acts as a cocatalyst which facilitates the photoexcited electrons transfer from $LaPO_4$ to Pt nanoparticles, and prevents the recombination of photoexcited electrons and holes. This is confirmed experimentally as shown in Fig. 8. The better charge separation enhances the efficiency of photocatalytic CO_2 conversion. Moreover, the Pt cocatalyst functions not only as photogenerated electron sink but also as CO_2 adsorber, since the $LaPO_4$–Pt sample shows larger CO_2 adsorption amounts, lower isosteric heat of CO_2 adsorption, although smaller specific surface area than bare $LaPO_4$, which thus accelerates the eight-electron reduction of CO_2 with H_2O into CH_4 (Eq. (5)) to proceed, and enhances the conversion selectivity of CO_2 reduction into CH_4. A detailed illustration of this mechanism is shown in Scheme 1.

4. Conclusions

In summary, hexagonal $LaPO_4$ nanorods have been successfully synthesized by hydrothermal method. The prepared $LaPO_4$ samples showed superior photocatalytic performance for CO_2 reduction with H_2O under mild conditions, and the main reduction products were CH_4 and H_2. The deposited Pt cocatalyst improved the photocatalytic activity and the selectivity for CH_4 formation. The maximum CH_4 and H_2 production rates were observed for

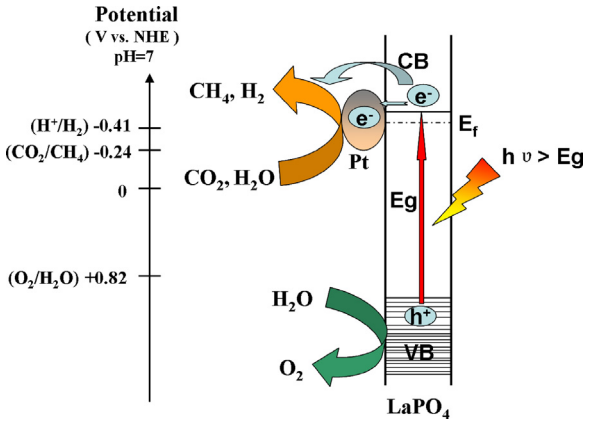

Scheme 1. Proposed mechanism of the photocatalytic CO_2 reduction over $LaPO_4$ photocatalyst with Pt cocatalyst in the presence of H_2O.

$LaPO_4$–1 wt%Pt, which was 5.6 and 2.8 times as high as that of $LaPO_4$ respectively, with the apparent quantum yield (AQY) increased by 5 times, and the selectivity for CH_4 formation achieved 100% as Pt content increased to 3 wt%. The enhanced photocatalytic activity and selectivity of Pt-deposited $LaPO_4$ can be attributed to the outstanding ability of the deposited Pt nanoparticles as an excellent electron transfer mediator and adsorber for CO_2. This work introduces $LaPO_4$ as a novel photocatalyst to convert CO_2 into chemicals, and indicates that the deposition of Pt is a good strategy to improve the activity and selectivity of $LaPO_4$ for photocatalytic CO_2 reduction.

Acknowledgments

This work is financially supported by the NSFC (Grants Nos. 20873022, U1305242, 21173044, and 21373050) and the National Key Basic Research Program of China (973 Program: 2013CB632405, 2014CB239303 and 2014CB260410).

Appendix A. Supplementary data

Supplementary data associated with this article can be found, in the online version, at http://dx.doi.org/10.1016/j.apcatb.2014.12.046.

References

[1] A.M. Omer, Renew. Sustain. Energy Rev. 12 (2008) 2265–2300.
[2] Y. Ma, X. Wang, Y. Jia, X. Chen, H. Han, C. Li, Chem. Rev. 114 (2014) 9987–10043.

[3] N.M. Dimitrijevic, B.K. Vijayan, O.G. Poluektov, T. Rajh, K.A. Gray, H. He, P. Zapol, J. Am. Chem. Soc. 133 (2011) 3964–3971.
[4] O.K. Varghese, M. Paulose, T.J. LaTempa, C.A. Grimes, Nano Lett. 9 (2009) 731–737.
[5] Q. Zhang, T. Gao, J.M. Andino, Y. Li, Appl. Catal. B: Environ. 123–124 (2012) 257–264.
[6] S. Xie, Y. Wang, Q. Zhang, W. Fan, W. Deng, Y. Wang, Chem. Commun. 49 (2013) 2451–2453.
[7] J. Yu, J. Low, W. Xiao, P. Zhou, M. Jaroniec, J. Am. Chem. Soc. 136 (2014) 8839–8842.
[8] Z. Wang, K. Teramura, S. Hosokawa, T. Tanaka, Appl. Catal. B: Environ. 163 (2015) 241–247.
[9] Q. Liu, Y. Zhou, J. Kou, X. Chen, Z. Tian, J. Gao, S. Yan, Z. Zou, J. Am. Chem. Soc. 132 (2010) 14385–14387.
[10] S.C. Yan, S.X. Ouyang, J. Gao, M. Yang, J.Y. Feng, X.X. Fan, L.J. Wan, Z.S. Li, J.H. Ye, Y. Zhou, Z.G. Zou, Angew. Chem. Int. Ed. 49 (2010) 6400–6404.
[11] Y. Xu, M.A.A. Schoonen, Am. Mineral. 85 (2000) 543–556.
[12] B. Pan, Q. Xie, H. Wang, J. Zhu, Y. Zhang, W. Su, X. Wang, J. Mater. Chem. A 1 (2013) 6629–6634.
[13] Q. Xie, Y. Wang, B. Pan, H. Wang, W. Su, X. Wang, Catal. Commun. 27 (2012) 21–25.
[14] D. Meziani, A. Reziga, G. Rekhila, B. Bellal, M. Trari, Energy Convers. Manage. 82 (2014) 244–249.
[15] H. Kim, D. Hwang, S. Bae, J. Jung, J. Lee, Catal. Lett. 91 (2003) 193–198.
[16] S.E. Siporin, B.C. McClaine, R.J. Davis, Langmuir 19 (2003) 4707–4713.
[17] S. Wang, S. Yan, X. Ma, J. Gong, Energy Environ. Sci. 4 (2011) 3805–3819.
[18] K. Riwotzki, H. Meyssamy, H. Schnablegger, A. Kornowski, M. Haase, Angew. Chem. Int. Ed. 40 (2001) 573–576.
[19] M. Yu, J. Lin, J. Fu, H.J. Zhang, Y.C. Han, J. Mater. Chem. 13 (2003) 1413–1419.
[20] L. Yu, H. Song, S. Lu, Z. Liu, L. Yang, X. Kong, J. Phys. Chem. B 108 (2004) 16697–16702.
[21] I.H. Tseng, J.C.S. Wu, H.-Y. Chou, J. Catal. 221 (2004) 432–440.
[22] J.L.C. Rowsell, O.M. Yaghi, J. Am. Chem. Soc. 128 (2006) 1304–1315.
[23] G. Halasi, G. Schubert, F. Solymosi, J. Phys. Chem. C 116 (2012) 15396–15405.
[24] D.F. Mullica, W.O. Milligan, D.A. Grossie, G.W. Beall, L.A. Boatner, Inorg. Chim. Acta 95 (1984) 231–236.
[25] V. Petruševski, B. Šoptrajanov, J. Mol. Struct. 115 (1984) 343–346.
[26] Y. Wang, Y. Wang, R. Xu, J. Phys. Chem. C 117 (2012) 783–790.
[27] D. Barreca, A. Gasparotto, C. Maragno, E. Tondello, E. Bontempi, L.E. Depero, C. Sada, Chem. Vap. Deposition 11 (2005) 426–432.
[28] D. Barreca, A. Gasparotto, C. Maragno, E. Tondello, Surf. Sci. Spectra 11 (2004) 52–58.
[29] E. Bêche, P. Charvin, D. Perarnau, S. Abanades, G. Flamant, Surf. Interface Anal. 40 (2008) 264–267.
[30] S. Zhang, S. Zhang, L. Song, Appl. Catal. B: Environ. 152–153 (2014) 129–139.
[31] J. Yu, K. Wang, W. Xiao, B. Cheng, Phys. Chem. Chem. Phys. 16 (2014) 11492–11501.
[32] Y. Pan, J.M. Zhang, W.M. Guan, K.H. Zhang, S. Chen, J. Phys. Chem. Solids 72 (2011) 1–4.
[33] J. Zhang, X. Chen, K. Takanabe, K. Maeda, K. Domen, J.D. Epping, X. Fu, M. Antonietti, X. Wang, Angew. Chem. Int. Ed. 49 (2010) 441–444.
[34] V. Spagnol, E. Sutter, C. Debiemme-Chouvy, H. Cachet, B. Baroux, Electrochim. Acta 54 (2009) 1228–1232.
[35] A. Ishikawa, T. Takata, J.N. Kondo, M. Hara, H. Kobayashi, K. Domen, J. Am. Chem. Soc. 124 (2002) 13547–13553.
[36] Y. Zhang, Z.-R. Tang, X. Fu, Y.-J. Xu, ACS Nano 5 (2011) 7426–7435.
[37] D.M. Pimpalshende, S.J. Dhoble, Luminescence (2014), http://dx.doi.org/10.1002/bio.2705.
[38] A.A. Bagatur'yants, I.M. Iskandarova, A.A. Knizhnik, V.S. Mironov, B.V. Potapkin, A.M. Srivastava, T.J. Sommerer, Phys. Rev. B: Condens. Matter 78 (2008) 165125.